

Research Article

Direct heating pattern on graphene oxide film to build flexible micro-supercapacitors



Cheng Peng^a, Qiang Li^{a,*}, Liang Niu^a, Hong Yuan^b, Jiahui Xu^b, QingQing Yang^a, YuanJun Yang^a, Guoxiang Li^a, Yanwu Zhu^{b,**}

^a School of Electronic Science and Applied Physics, Hefei University of Technology, Hefei, Anhui, 230009, China

^b Hefei National Research Center for Physical Sciences at the Microscale, CAS Key Laboratory of Materials for Energy Conversion & Department of Materials Science and Engineering, University of Science and Technology of China, Hefei, Anhui, 230026, PR China

ARTICLE INFO

Article history:

Received 25 November 2020

Received in revised form

28 December 2020

Accepted 28 December 2020

Available online 4 January 2021

Keywords:

Micro-supercapacitor

Heating pattern

Graphene oxide film

Flexible

High performance

ABSTRACT

The development of portable and wearable electronic devices continues to increase the demand for miniature energy storage units. Here, we fabricate the flexible micro-supercapacitors (MSCs) through direct heating pattern on graphene oxide film. The shape designable MSCs are based on planar reduced graphene oxide/graphene oxide (rGO/GO) structure, with rGO as electrode and GO as separator. The GO area heated by heating pen is reduced to rGO, and the area with no heating is still GO. The interdigitated MSC made at 400 °C delivers high area capacitance of 94.8 mF cm⁻² at current density of 0.25 mA cm⁻² within poly(vinyl alcohol) (PVA)/H₂SO₄ gel electrolyte. It provides high energy density of 10.7 mWh cm⁻² at power density of 112.6 mW cm⁻². In addition, it also has excellent mechanical stability, with basically unchanged area capacitance from 0° to 180° bending angles. The MSCs with shapes of spiral, concentric circle and eight-trigrams are also fabricated via this method. The results indicate that heating pattern on GO films to build flexible MSC is a promising and low-cost new method to fabricate energy storage equipment for future electronic devices.

© 2021 Elsevier Ltd. All rights reserved.

1. Introduction

Flexible energy storage equipment is considered to be new energy supply system to meet the needs of various portable and wearable electronic devices [1–3]. Flexible micro-supercapacitors (MSCs) have attracted widespread attention due to their excellent mechanical properties, high power density, fast charge/discharge rates, and great cycle stability when used as energy storage equipment [4–6]. Reduced graphene oxide (rGO) with large specific surface area, excellent conductivity and mechanical flexibility is an ideal candidate electrode material for flexible MSCs [7–9]. Especially, planar rGO film demonstrates great potential in future electronic applications [10–12]. The traditional flexible supercapacitors are usually assembled by two electrodes filled with electrolyte on flexible substrates, plus an essential porous membrane or solid electrolyte separator, which leads to complex processing procedures and relatively high manufacturing costs [13,14].

Therefore, the development of easily manufactured and process-simple flexible MSCs without sacrificing other electrochemical properties is a crucial challenge [15].

The most common strategy to make flexible MSCs is to use photolithography to produce interdigitated patterns with electrode materials on flexible films [16–18]. Other fabrication methods such as ink printing [19–21], screen printing [22–24], plasma etching [25–27] and stamping [28,29] have also been developed to build flexible interdigitated MSCs on many kinds of substrates. In recent years, laser processing has been found to be an attractive technology for fabricating MSCs because of its substrate-free, flexible and efficient nature [30–32]. Laser scribing on graphene oxide (GO) film can directly build rGO/GO alternate arrangement for flexible MSCs [33,34]. The laser has the ability to reduce GO to highly conductive rGO, allowing the convenient and non-toxic fabrication of rGO/GO pattern in a variety of configurations [35–38]. In this way, the electrode (rGO) and separator (GO) can be reasonably integrated into one film without additional adhesive or assembly process, resulting in the flexible MSCs themselves fabricated directly on GO film [39,40]. When the electrically insulating GO layers absorb water from hydrated electrolyte, it would change to

* Corresponding author.

** Corresponding author.

E-mail addresses: qli@hfut.edu.cn (Q. Li), zhuyanwu@ustc.edu.cn (Y. Zhu).

an excellent ionic conductor but still electrical insulator, which makes the possibility of its use as electrode separator [40]. These kinds of MSCs also inherit the mechanical properties of GO films, while still maintaining high capacitance performance [35].

However, the laser scribing on GO film to make MSCs extremely depends on laser equipment, accompanying the disadvantages of long production cycle and high production cost [41–43]. The limited reduction depth of GO to rGO, due to the reflection of laser by rGO layers on the surface of GO film, may also prevent the improvement of energy density [44]. Therefore, in this study, we firstly, to the best of our knowledge, try to fabricate flexible MSCs by direct heating pattern on GO film. Here, the laser equipment is replaced by a heating pen, and the high temperature pen tip can replace laser to reduce GO to rGO. We directly use the heating pen to draw patterns on GO film, just like using a pen to write on paper. Therefore, it is very convenient to get the desired shapes. The GO area heated by the high temperature heating pen tip would be reduced to rGO, and the area with no heating is still GO. The flexible MSCs are fabricated based on planar interdigitated rGO/GO structure, with rGO working as electrode and GO as separator. The MSC made by heating pen tip at 400 °C delivers high area capacitance of 94.8 mF cm⁻² at current density of 0.25 mA cm⁻² within poly(vinyl alcohol) (PVA)/H₂SO₄ gel electrolyte. It provides high energy density of 10.7 mWh cm⁻² at power density of 112.6 mW cm⁻². In addition, it also has excellent mechanical stability, with basically unchanged area capacitance from 0° to 180° bending angles. This heating pattern method can also easily make MSCs with other shapes, such as spiral, concentric circle and eight-trigrams. Therefore, the direct heating pattern on GO films to build flexible MSCs is a promising and low-cost new method to fabricate flexible energy storage equipment for future electronic devices.

2. Experimental

2.1. Materials

The GO film was obtained from the Changzhou Fuxi Technology Co. Ltd, China. Heating pen and conductive silver paste were commercially available from supermarkets. H₂SO₄, PVA and ethanol were analytical pure grade and purchased from Sinopharm Chemical Reagent Co. Polyvinyl alcohol was purchased from Aladdin. Deionized water was used for all the experiment processes.

2.2. Fabrication of MSCs on GO film

The fabrication process to build MSCs on GO film by direct heating pattern is schematically illustrated in Fig. 1. GO film was cut into desired shape and placed on the experimental table. Turn on the heating pen and set it to desired temperature. When the heating pen tip (Fig. 1d) reached the set temperature (Fig. 1c), we can hold the heating pen to draw the desired shapes of MSCs on GO film by hand, as shown in Fig. 1a. The change of GO film cross section after drawing by the high temperature heating pen tip was schematically illustrated in Fig. 2b. Next, a slice of copper sheet was connected to the rGO electrode by conductive silver paste. The PVA/H₂SO₄ gel electrolyte was dropped on MSCs and dried at room temperature for 48 h. After then, the MSCs were sealed with transparent tape. The PVA/H₂SO₄ gel electrolyte was prepared by mixing 6g H₂SO₄ and 6g PVA in 60 ml deionized water and heated up to 90 °C for 1 h under vigorous stirring [45]. The MSCs obtained by heating pattern on GO film were called TGF, and the TGF-360, TGF-400, TGF-440, and TGF-480 corresponds to the interdigitated MSCs (Fig. 1e) made by 360, 400, 440 and 480 °C heating pen tip, respectively. The other three MSCs with shapes of spiral (S-TGF,

Fig. 1f), concentric circle (C-TGF, Fig. 1g), and Eight Diagrams (E-TGF, Fig. 1h) were fabricated using the same method by heating pen tip at 400 °C. The mass loadings of these rGO/GO micro-supercapacitors are between 14.6 mg cm⁻² and 12.4 mg cm⁻².

2.3. Structural characterizations

The morphologies and microstructures of the prepared samples were examined with tungsten filament scanning electron microscopy (SEM, KYKY-EN6200/6900). The powder X-ray diffraction (XRD, ESCALAB 250xi) with Bragg's angle (2θ) range from 5° to 60° was used to determine the structures of the samples. The surface properties of the samples were analyzed by X-ray photoelectron spectroscopy (XPS, ESCALAB 250Xi). Raman spectra (LabRAM HR Evolution) were recorded from 1200 to 1800 cm⁻¹.

2.4. Electrochemical measurements

The cyclic voltammetry (CV), galvanostatic charge-discharge (GCD) and electrochemical impedance spectroscopy (EIS) were measured with electrochemical workstation (CHI660E, Chenhua Instruments, China). Within PVA/H₂SO₄ electrolyte, the potential window was controlled at 0–1 V, and the impedances were recorded over 0.01–100,000 Hz with an AC perturbation of 5 mV. The specific area capacitance (C) was calculated from the GCD curves at different current densities based on the following equation:

$$C = \frac{I \Delta t}{\Delta V} \quad (1)$$

where I is the discharge current (A), Δt is the discharge time (s), S is total area of the MSC, and ΔV is the operating voltage range (minus the IR voltage drop).

The area energy density (E) and area power density (P) were obtained from the following equation:

$$E = \frac{C \Delta V^2}{2 \times 3600} \quad (2)$$

$$P = \frac{3600E}{\Delta t} \quad (3)$$

where C is the area capacitance, Δt is the discharge time.

3. Results and discussion

3.1. Material characterizations

Fig. 2 shows SEM images of the surface and cross section of TGF-X (TGF-X represents TGF-360, TGF-400, TGF-440 and TGF-480). The GO/rGO junction area separated with dashed yellow line on the surface of TGF-400 is shown in Fig. 2a. It is obvious that there are certain amounts of wrinkles on the surface of GO film (Fig. 2a and Fig. S1a). The interphase line between rGO and GO is very clear, with GO on the left side and rGO on the right side. After reducing GO to rGO by the high temperature heating pen, the surface wrinkles of GO films disappear, resulting in some cracks on rGO flat surface (Fig. 2a and Fig. S1b). The high temperature heating pen tip would also smooth the surface wrinkles of GO film when sliding on its surface. Fig. 2b and c shows the cross section images of GO/rGO film in TGF-400, which demonstrates clearly the expansion when GO was reduced to rGO. Through the panoramic cross section view of GO/rGO (Fig. 2b), we can see the rGO structure with a lower center and higher two sides. The downward pressure of the heating

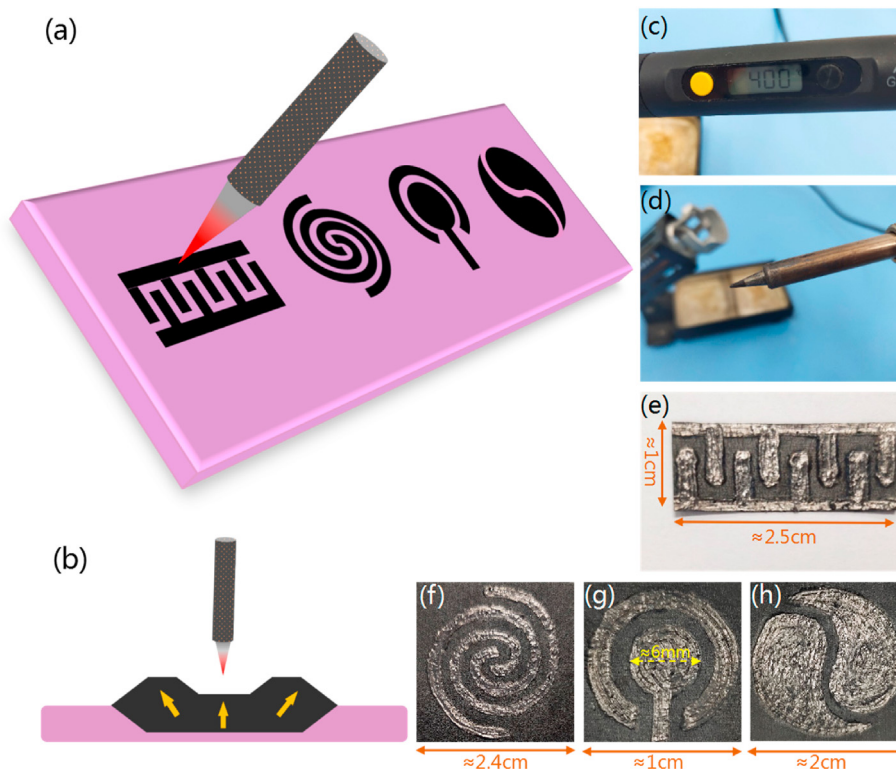


Fig. 1. The fabrication process to build MSCs by direct heating pattern on GO film. (a) Schematic illustration of drawing the designed MSCs on the surface of GO film by a heating pen. (b) Schematic illustration to show the change of GO film cross section after drawing by the high temperature heating pen tip. (c) Setting the temperature of heating pen tip. (d) The tip of the heating pen. (e–h) The photo images of interdigitated (TGF-X), spiral (S-TGF), concentric circle (C-TGF) and eight diagrams (E-TGF) MSCs, respectively. The width and length of TGF-X are 1 cm and about 2.5 cm, and their total areas are about 2.5 cm². The overall diameter of S-TGF is about 2.4 cm. The inner circle diameter and the outer circle diameter of C-TGF are about 6 mm and 1 cm. The overall diameter of E-TGF is about 2 cm. (A colour version of this figure can be viewed online.)

pen tip during high temperature reduction process limits the expansion of the rGO layers directly under the heating pen tip at some extent, and the rGO layers beside the heating pen tip would expand more freely. The enlarged SEM image of GO/rGO junction area of TGF-400 shows that the thickness of GO film is about 90 μm , and the thickness of rGO film would expand to 120–200 μm (Fig. S1c). During heating pattern process, lots of water vapor and CO₂ were instantaneously produced when GO was reduced to rGO, which leads to the expansion of rGO layers. The specially enlarged rGO part (Fig. 2c) indicates that the rGO layers have been completely opened, and the reduction depth has almost reached the bottom of the film. However, the reduction depth of TGF-360, TGF-440 and TGF-480 is not as deep as that of TGF-400, as shown in Fig. 2d–f. For TGF-360 (Fig. 2d and Fig. S1d), because of the expansion of the surface rGO layers, the lower temperature gradient prevents the heat from being effectively transmitted to the bottom layers of GO film to reduce GO to rGO. When the temperature of heating pen tip is too high, for example fabricating TGF-440 (Fig. 2e and Fig. S1e) and TGF-480 (Fig. 2f and Fig. S1f), the reduction speed of GO is very fast, and the rGO layers tend to crack easily. Therefore, it is necessary to accelerate the sliding speed of the heating pen tip, which would lead to the heating time actually reduced. In this condition, when the upper parts of GO layers have been reduced and expanded, and even cracked dramatically (Fig. 2e and f), but the heat has not transmitted effectively to the bottom parts of GO film to reduce the GO layers.

Fig. 3a shows the XRD spectra of GO and rGO in TGF-X. One sharp peaks around 11.44° can be detected, corresponding to the (002) plane of graphene oxide. After rapid reduction during heating pattern process, large amounts of oxygen-containing functional

groups in GO were decomposed. Therefore, the peak intensities of rGO dropped significantly, and that in TGF-400 dropped the most. At the same time, the peak positions of TGF-X shifted slightly to the right, mainly due to the fact that the distance between the (002) planes of GO decreased after reduction of GO. Raman spectroscopy is another powerful tool for evaluating the chemical structure of GO and rGO. As shown in Fig. 3b, the typical Raman spectra of GO and rGO in TGF-X present two prominent peaks located at 1350 and 1590 cm^{-1} , which correspond to the D band and G band of the graphitic carbon, respectively. The D band is attributed to the defect and disordered structure, while the G band corresponds to the crystalline graphite carbon [46]. The relative intensity ratio (ID/IG) of D peak to G peak is usually used to quantify the defects existed in the graphite material [47]. The ID/IG ratio of GO was calculated to be 1.14, and the ID/IG ratios of TGF-360, TGF-400, TGF-440, and TGF-480 increased to 1.21, 1.22, 1.21, and 1.18, respectively. The increases of ID/IG ratio indicate the introduction of more defects into rGO layers when GO was reduced to rGO during heating pattern process, which would benefit the electrochemical performances of TGF-X. Obviously, TGF-400 has the highest ID/IG ratio among TGF-X.

Fig. 3c shows the XPS spectra of GO and rGO in TGF-X. According to the binding energy of the peaks presented in the XPS spectra, they are mainly assigned to C1s and O1s. The nitrogen existed between GO layers from air may bond with carbon atoms during heating pattern processes at high temperature, which leads to the weak N1s peaks observed in the XPS spectra of rGO in TGF-X. The oxygen and nitrogen doping into rGO electrodes would introduce the pseudocapacitance to further improve the electrochemical performances of TGF-X [48,49]. The C/O ratio of GO is 1.30, and after

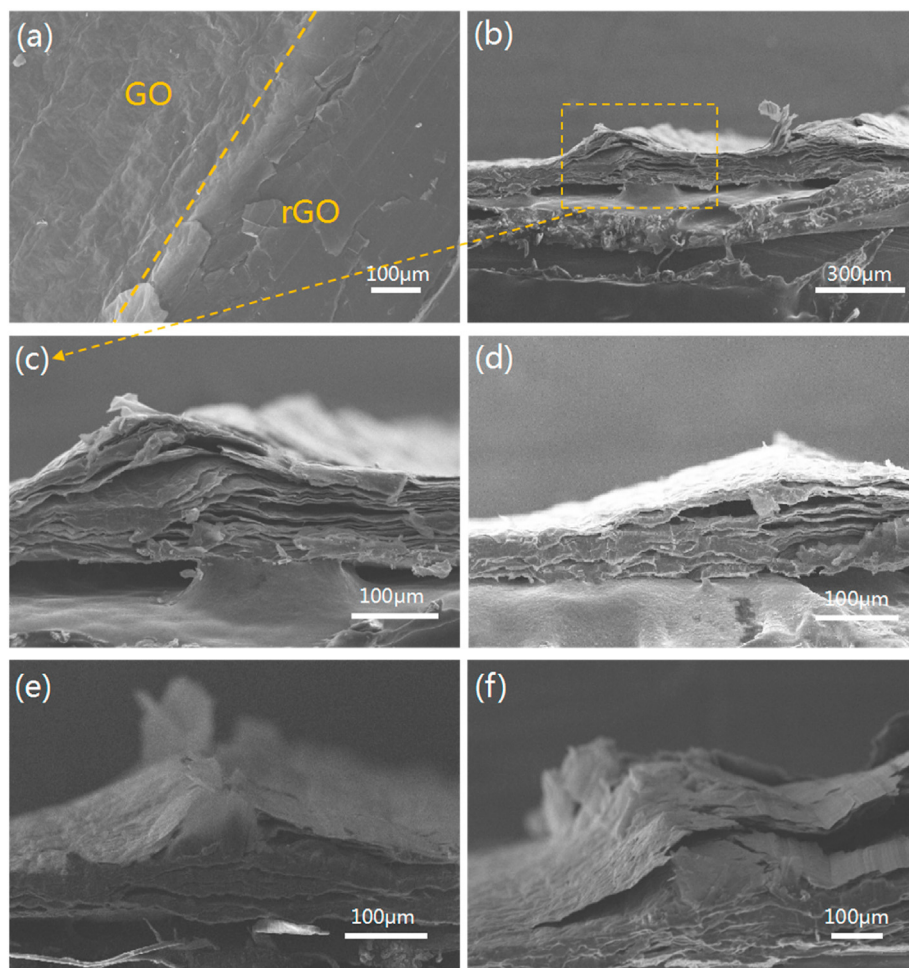


Fig. 2. SEM images of surface and cross section of TGF-X. (a) Surface of GO/rGO junction area in TGF-400. (b) Cross section of TGF-400. (c) Enlarged cross section of the area in (b). (d–f) Cross sections of TGF-360, TGF-440 and TGF-480, respectively. (A colour version of this figure can be viewed online.)

thermal reduction, the C/O ratio of rGO in TGF-360, TGF-400, TGF-440 and TGF-480 increases to 1.54, 1.68, 1.65 and 1.76, respectively. The main reason for the increase of C/O from GO to rGO in TGF-X is the decomposition of part oxygen-containing functional groups in GO during heating pattern processes. The peak of C1s ranges are broad from 282 to 292 eV, which is composed of several carbons in different functional groups (esters, ketones, oximes or carboxyl groups) [50]. Fig.3d and Fig.S2 are deconvolution results of C1s peaks from GO and rGO in TGF-X, respectively. The primary peak of C1s appears at 284.7 eV, which is attributed to graphitic carbon. Other smaller peaks were identified as C–O at 285.4 eV, C=O at 286.7 eV, and O–C=O at 288.7 eV. It is obvious that the intensity of C=O decreases while the intensity of C–O increases from GO (Fig. S2a) to rGO (Fig.3d and Fig. S2b–2d), which is also mainly caused by the decomposition of oxygen-containing functional groups during thermal reduction of GO.

3.2. Electrochemical characterization

Electrochemical performances of the TGF-X are shown in Fig. 4. Fig. 4a shows their CV curves at scan rate of 20 mV s^{-1} with voltage window of 0–1 V. The TGF-400 has the largest CV integrating area among the TGF-X, which indicates its highest specific area capacitance. The GCD curves of TGF-X at 0.25 mA cm^{-2} from 0 to 1V were also tested to further clarify their specific capacitance (Fig. 4b).

Obviously, the area capacitance performance of TGF-400 is much better than those of TGF-360, TGF-440 and TGF-480. The area capacitance performances indicated by the GCD and CV test results have excellent correspondence. The distortion of CV curves from rectangular shape and GCD curves from triangular shape is mainly caused by the high internal ions conductive resistance in TGF-X. The pseudocapacitance introduced by the oxygen and nitrogen doping into rGO electrodes (XPS spectra of TGF-X in Fig. 3c) during heating pattern process may also contribute to this distortion. Calculated according to the discharge parts of GCD curves, the area capacitances of TGF-360, TGF-400, TGF-440 and TGF-480 at 0.25 mA cm^{-2} are 47.9, 94.8, 54.7 and 31.9 mF cm^{-2} , respectively. Fig. 4c shows the area capacitances of TGF-360, TGF-400, TGF-440 and TGF-480 within PVA/H₂SO₄ electrolyte at current density from 0.25 to 1 mA cm^{-2} . Obviously, TGF-400 has the highest area capacitance among TGF-X at all current densities. From 0.25 to 1 mA cm^{-2} , the capacitance retentions of TGF-360, TGF-400, TGF-440 and TGF-480 are 49.3%, 58.3%, 35.2% and 27.5%, respectively, which also demonstrates the best rate capability of TGF-400. The deepest reduction depth of GO layers to rGO layers in TGF-400 (Fig. 2 and Fig.S1) may be the main reason for its highest area capacitance among TGF-X. The highest ID/IG ratio of TGF-400 (1.22) among TGF-X (1.21, 1.21, and 1.18 for TGF-360, TGF-440 and TGF-480, respectively) may also contribute to its best capacitance performance.

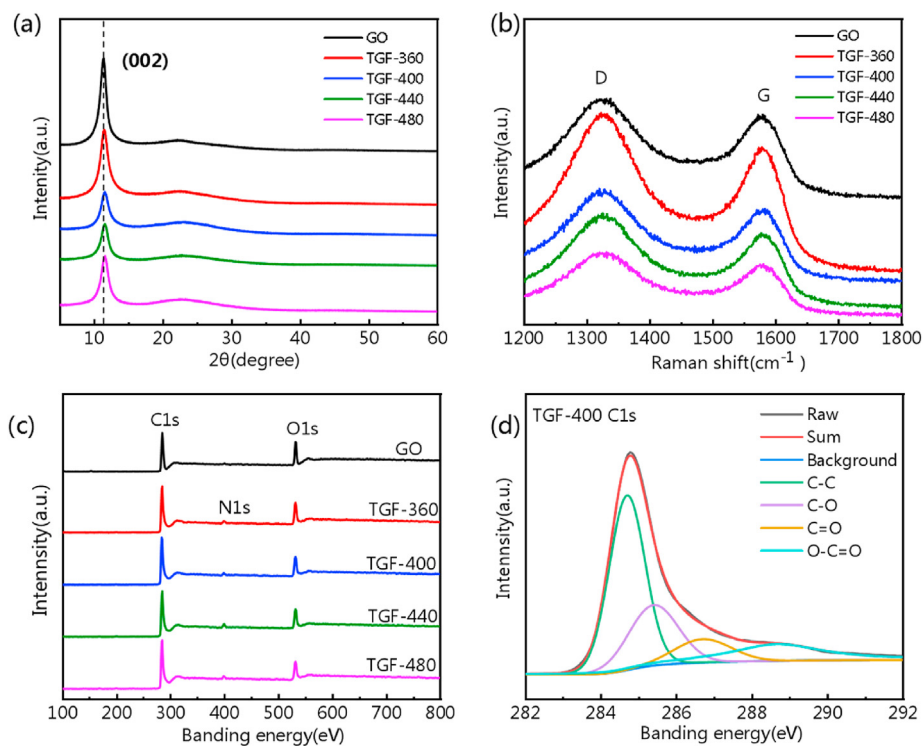


Fig. 3. (a) XRD spectra, (b) Raman spectra and (c) XPS spectra of GO and rGO in TGF-X. (d) C 1s spectrum of XPS survey of rGO in TGF-400. (A colour version of this figure can be viewed online.)

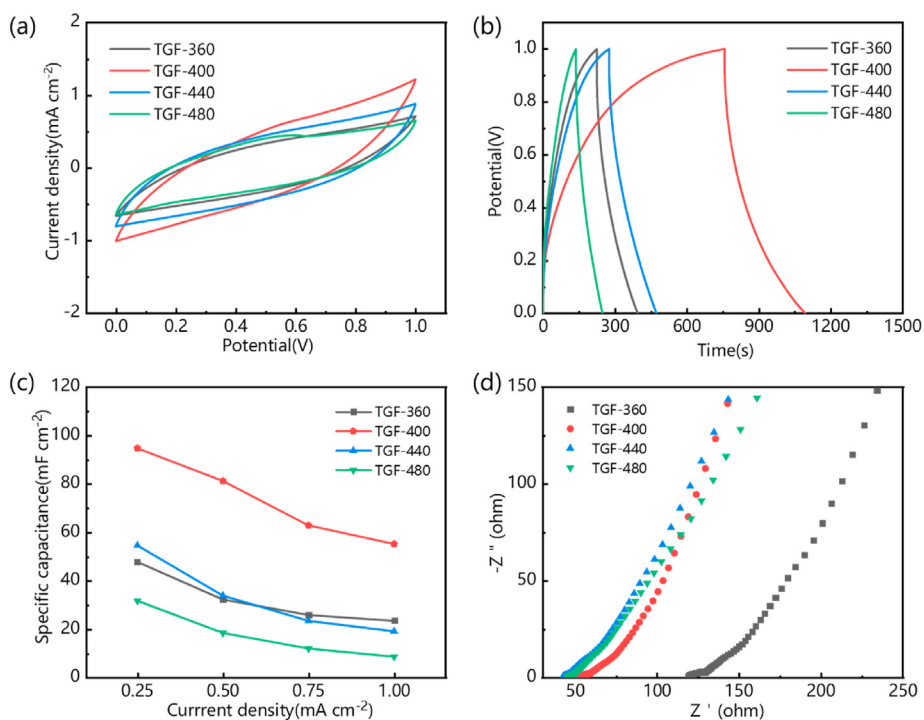


Fig. 4. Electrochemical performances of TGF-X with PVA/H₂SO₄ as electrolyte. (a) CV curves at 20 mV s⁻¹. (b) GCD curves at 0.25 mA cm⁻². (c) Specific area capacitances calculated from the discharge curves of GCD under different current densities. (d) Nyquist plots. (A colour version of this figure can be viewed online.)

Electrochemical Impedance Spectroscopy (EIS) data of the TGF-X were collected to demonstrate their electronic and ionic conductivity behavior (Nyquist plots, Fig. 4d.). The intercept of Nyquist plots of TGF-X with real axis indicates their equivalent serial

resistance (ESR). The ESRs of TGF-400, TGF-440 and TGF-480 are about 50 Ω, which are lower than that of TGF-360 (~120Ω), indicating that the 360 °C during our heating pattern process is not high enough to reduce GO to rGO well. TGF-400 has a shorter length of

45° sloped line (warburg impedance) than those of TGF-360, TGF-440 and TGF-480, which indicates the best electrolyte ions diffusion ability of TGF-400 with PVA/H₂SO₄ as electrolyte among TGF-X [51].

The electrochemical performance of TGF-400 was further analyzed, as shown in Fig. 5. Both CV curves at scan rates from 20 to 500 mV s⁻¹ (Fig. 5a) and GCD curves at current densities from 0.25 to 1 mA cm⁻² (Fig. 5b) illustrate the mainly typical electrical double layer capacitance (EDLC) behavior of TGF-400. Fig. 5c shows its area capacitances at different current densities calculated from the GCD discharge curves. Obviously, the area capacitance increases with the decrease of current density, due to the longer absorbing/desorbing time at lower current density. At 0.25 mA cm⁻², the area capacitance can reach up to 94.8 mF cm⁻², and it still keeps 55.3 mF cm⁻² at 1 mA cm⁻², indicating the excellent rate performance of TGF-400. In order to evaluate the bending stability of TGF-400, its CV performances under different bend angles were tested (Fig. 5d). The bend angles from 0 to 180° have almost no effect on the CV curves, which demonstrates that the rGO/GO layers in TGF-400 can keep their excellent mechanical stability well. Therefore,

our heating pattern method to directly fabricate flexible MSCs on GO film has potential practical application value for fabricating flexible electronic devices.

The charging/discharging stability of TGF-400 was investigated by performing GCD test at 0.5 mA cm⁻² for 20,000 cycles (Fig. 5e). In the first 2000 cycles, the capacitance retention can maintain 100%. From 2000 to 6000 cycles, it keeps dropping to 71.4%, and maintaining this retention to 11,000 cycles. In the last 13,000–20,000 cycles, the capacitance can still keep 57.1% of the original one. Therefore, as a whole, TGF-400 maintains excellent cycling stability. Although the oxygen doping in rGO/GO layers of TGF-400 is high (Fig. 3c), it might have no deleterious effect on the cycling performance [52]. The decrease of cycling stability is mainly due to the structural damage of TGF-400 during charging/discharging process. Ragone plots of TGF-400 are demonstrated to further obtain its overall performance (Fig. 5f). The area energy density of TGF-400 can reach up to 10.7 mWh cm⁻² at area power density of 112.6 mW cm⁻², which is comparable or superior to some recently reported MSCs [24,30,53–58], such as the MSC patterned by laser scribing on graphene film (0.92 μWh cm⁻² at

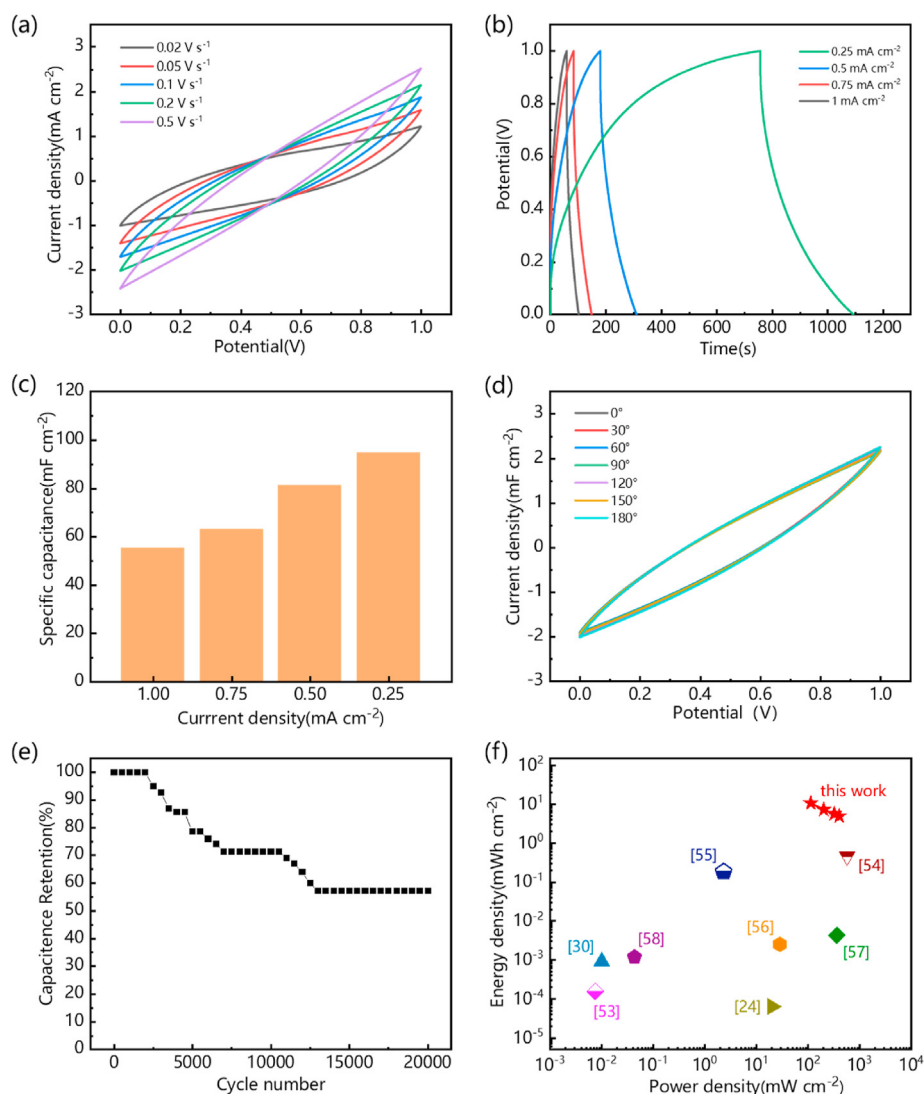


Fig. 5. Electrochemical performance of TGF-400 with PVA/H₂SO₄ as electrolyte. (a) CV curves at different scan rates and (b) GCD curves at different current densities from 0 to 1 V. (c) specific area capacitances calculated from the discharge curves of GCD under different current densities. (d) Bending stability at different bend angles. (e) Charging/discharging stability for 20,000 cycles at 0.5 mA cm⁻². (f) Ragone plots of TGF-400 compared with other reported MSCs. (A colour version of this figure can be viewed online.)

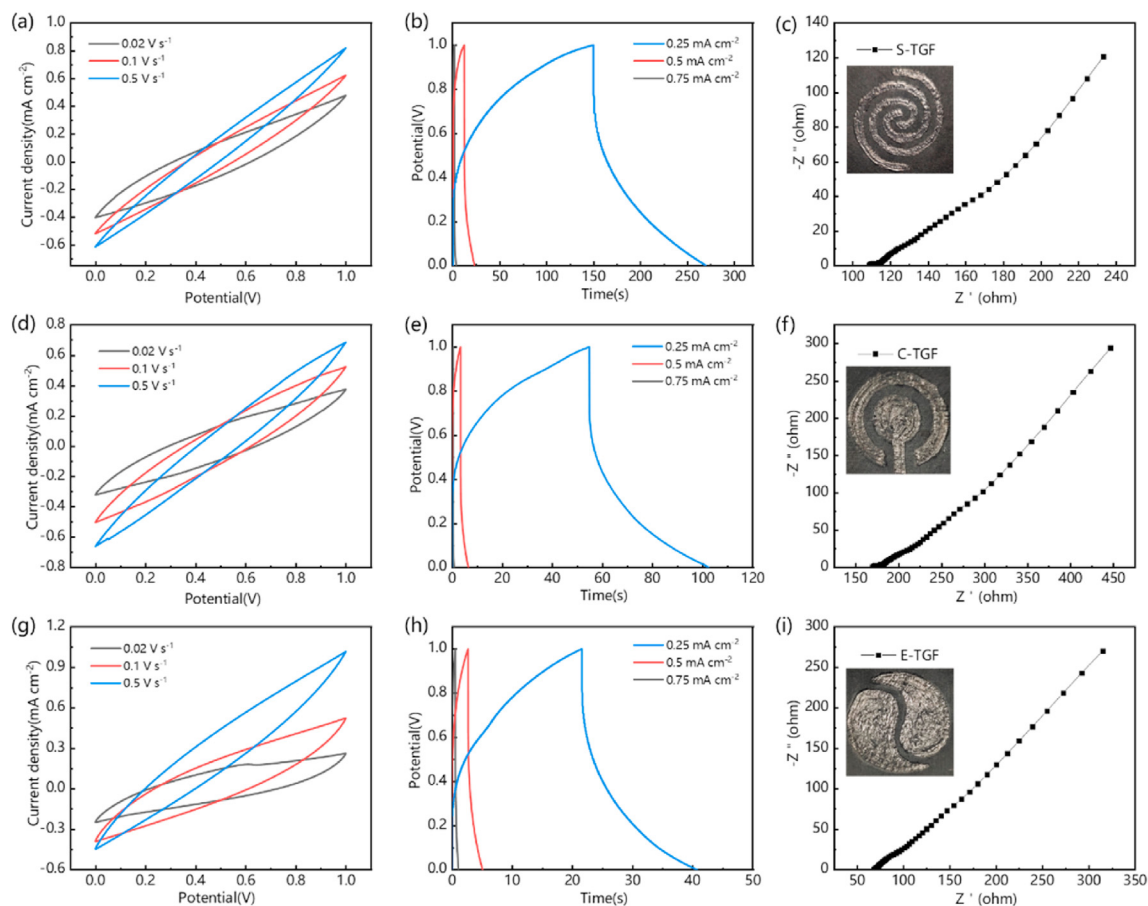


Fig. 6. Electrochemical performances of S-TGF, C-TGF and E-TGF measured with PVA/H₂SO₄ as electrolyte. (a–c) CV curves, GCD curves and EIS plot of S-TGF. (d–f) CV curves, GCD curves and EIS plot of C-TGF. (g–i) CV curves, GCD curves and EIS plot of E-TGF. The insets in (a), (f) and (i) are the photo images of S-TGF, C-TGF and E-TGF, respectively. (A colour version of this figure can be viewed online.)

10 $\mu\text{Wh cm}^{-2}$ [36], laser patterned graphene MSC (0.46 mWh cm^{-2} at 570 mW cm^{-2}) [54], and hybrid MSCs of Cu_{0.56}Co_{2.44}O₄@MnO₂//carbon nanotubes (182.3 $\mu\text{Wh cm}^{-2}$ at 2.3 mW cm^{-2}) [55] and PEDOT@rGO//PPy@rGO (4.3 $\mu\text{Wh cm}^{-2}$ at 360 mW cm^{-2}) [57] fabricated by photolithographic techniques.

In order to show the highly editable nature of the heating pattern method, we also designed and fabricated another three shapes of MSCs (spiral, concentric circle and eight trigrams) via direct heating pattern on GO film at 400 °C. Fig. 6 shows the electrochemical performances of S-TGF, C-TGF and E-TGF. The CV curves at 0.02–0.5 V s^{-1} , GCD curves at 0.25–0.75 mA cm^{-2} and EIS plots of S-TGF (Fig. 6a–c), C-TGF (Fig. 6d–f) and E-TGF (Fig. 6g–i) show their similar shapes with those of interdigitated TGF-X (TGF-400 for example), which demonstrates that the heating pattern method has universal applicability when fabricating MSCs with different shapes on GO film. Calculated according to the discharging part of GCD curves at 0.25 mA cm^{-2} , the area capacitances of S-TGF, C-TGF and E-TGF are 39.7, 14.1 and 6.3 mF cm^{-2} , respectively. The largest electrode-to-electrode relative area of S-TGF among the three MSCs (as shown in the insets of Fig. 6c, f and i) is main reason for its highest area capacitance. In industry, we can make a heating pen tip with various shapes or a heating metal device like a seal to fabricate flexible MSCs on GO film easily and efficiently. Therefore, the heating pattern method represents a new processing way to obtain flexible MSCs to meet the needs of various portable and wearable electronic devices.

4. Conclusions

In summary, we have successfully fabricated flexible MSCs via direct heating pattern on GO film. The interdigitated MSCs were built at four different temperatures, and 400 °C is the optimum temperature in our experiment to obtain MSC with area capacitance of 94.8 mF cm^{-2} at 0.25 mA cm^{-2} and energy density of 10.7 mWh cm^{-2} at 112.6 mW cm^{-2} . In addition, the area capacitance of this MSC keeps almost the same from 0° to 180° bending angles, showing its excellent mechanical stability. After 20,000 charging/discharging cycles, this MSC still maintains 57.1% of its initial area capacitance, indicating its excellent rate capability. Besides interdigitated MSC, other shapes of MSCs, such as spiral, concentric circle and eight-trigrams, are also easily fabricated through this heating pattern method. Therefore, compared to laser-scribing on GO film to make flexible rGO/GO MSCs, heating pattern method has easy controlled process and needs no sophisticated equipment, resulting in offering a simple and cost-effective way to fabricate miniature electronics.

CRedit authorship contribution statement

Cheng Peng: Investigation, Data curation, Writing–Original draft preparation. **Qiang Li:** Supervision, Formal analysis, Data curation, Writing - review & editing. **Liang Niu:** Investigation. **Hong Yuan:** Resources. **Jiahui Xu:** Resources. **QingQing Yang:** Investigation. **YuanJun Yang:** Formal analysis. **Guoxiang Li:** Formal analysis.

Yanwu Zhu: Conceptualization, Formal analysis, Writing - review & editing.

Declaration of competing interest

The authors declare that they have no known competing financial interests or personal relationships that could have appeared to influence the work reported in this paper.

Acknowledgements

This work was funded by the Natural Science Foundation of China (51772282, 51322204), the Fundamental Research Funds for the Central Universities (108-4115100092) and the Innovative Program of Development Foundation of Hefei Center for Physical Science and Technology (2018CXFX001).

Appendix A. Supplementary data

Supplementary data to this article can be found online at <https://doi.org/10.1016/j.carbon.2020.12.089>.

References

- [1] X. Wang, G. Shi, Flexible graphene devices related to energy conversion and storage, *Energy Environ. Sci.* 8 (2015) 790–823.
- [2] Z.J. Wang, H. Gao, Q. Zhang, Y.Q. Liu, J. Chen, Z.P. Guo, Recent advances in 3D graphene architectures and their composites for energy storage applications, *Small* 15 (2019) 1803858.
- [3] M. Beidaghi, Y. Gogotsi, Capacitive energy storage in micro-scale devices: recent advances in design and fabrication of micro-supercapacitors, *Energy Environ. Sci.* 7 (2014) 867–884.
- [4] P. Huang, C. Lethien, S. Pinaud, K. Brousse, On-chip and freestanding elastic carbon films for micro-supercapacitors, *Science* 351 (2014) 691–695.
- [5] D.P. Qi, Y. Liu, Z.Y. Liu, L. Zhang, X.D. Chen, Design of architectures and materials in in-plane micro-supercapacitors: current status and future challenges, *Adv. Mater.* 29 (2017) 1602802.
- [6] X.F. Wang, Y. Chen, O.G. Schmidt, C.L. Yan, Engineered nanomembranes for smart energy storage devices, *Chem. Soc. Rev.* 45 (2016) 1308–1330.
- [7] W.K. Chee, H.N. Lim, Z. Zainal, N.M. Huang, I. Harrison, Y. Andou, Flexible graphene-based supercapacitors: a review, *J. Phys. Chem. C* 120 (2016) 4153–4172.
- [8] C.Y. Wang, K.L. Xia, H.M. Wang, X.P. Liang, Z. Yin, Y.Y. Zhang, Advanced carbon for flexible and wearable electronics, *Adv. Mater.* 31 (2019) 1801072.
- [9] M.F. El-Kady, Y.L. Shao, R.B. Kaner, Graphene for batteries, supercapacitors and beyond, *Nat. Rev. Mater.* 1 (2016) 16033.
- [10] V. Georgakilas, J.N. Tiwari, K.C. Kemp, J.A. Permana, A.B. Bourlino, K.S. Kim, et al., Noncovalent functionalization of graphene and graphene oxide for energy materials, biosensing, catalytic, and biomedical applications, *Chem. Rev.* 116 (2016) 5464–5519.
- [11] X.H. Zhao, J.Q. E, G. Wu, Y.W. Deng, D.D. Han, B. Zhang, et al., A review of studies using graphenes in energy conversion, energy storage and heat transfer development, *Energy Convers. Manag.* 184 (2019) 581–599.
- [12] G. Eda, G. Fanchini, M. Chhowalla, Large-area ultrathin films of reduced graphene oxide as a transparent and flexible electronic material, *Nat. Nanotechnol.* 3 (2008) 270–274.
- [13] X.H. Lu, M.H. Yu, G.M. Wang, Y.X. Tong, Y. Li, Flexible solid-state supercapacitors: design, fabrication and applications, *Energy Environ. Sci.* 7 (2014) 2160–2181.
- [14] W. Liu, M.S. Song, B. Kong, Y. Cui, Flexible and stretchable energy storage: recent advances and future perspectives, *Adv. Mater.* 29 (2017) 1603436.
- [15] T. Kuila, A.K. Mishra, P. Khanra, N.H. Kim, J.H. Lee, Recent advances in the efficient reduction of graphene oxide and its application as energy storage electrode materials, *Nanoscale* 5 (2013) 52–71.
- [16] A. Tyagi, K.M. Tripathi, R.K. Gupta, Recent progress in micro-scale energy storage devices and future aspects, *J. Mater. Chem. A* 3 (2015) 22507–22541.
- [17] L.L. Liu, Z.Q. Niu, J. Chen, Design and integration of flexible planar micro-supercapacitors, *Nano Res.* 10 (2017) 1524–1544.
- [18] C.Y. Yu, J.N. An, Q. Chen, J.Y. Zhou, W. Huang, Y.J. Kim, et al., Recent advances in design of flexible electrodes for miniaturized supercapacitors, *Small Methods* 4 (2020) 1900824.
- [19] K. Guo, Y.H. Wan, N. Yu, L.T. Hu, T.Y. Zhai, H.Q. Li, Hand-drawing patterned ultra-thin integrated electrodes for flexible micro supercapacitors, *Energy Storage Mater.* 11 (2018) 144–151.
- [20] H.B. Hu, T. Hua, An easily manipulated protocol for patterning of MXenes on paper for planar micro-supercapacitors, *J. Mater. Chem. A* 5 (2017) 19639–19648.
- [21] J.T. Li, S.S. Deleka, P.P. Zhang, S. Yang, M.R. Lohe, X.D. Zhuang, et al., Scalable fabrication and integration of graphene micro-supercapacitors through full inkjet printing, *ACS Nano* 11 (2017) 8249–8256.
- [22] R.S. Guo, J.T. Chen, B.J. Yang, L.Y. Liu, L.J. Su, B.S. Shen, et al., In-plane micro-supercapacitors for an integrated device on one piece of paper, *Adv. Funct. Mater.* 27 (2017) 1702394.
- [23] L. Liu, Q. Lu, S.L. Yang, J. Guo, Q.Y. Tian, W.J. Yao, et al., All-Printed solid-state micro-supercapacitors derived from self-template synthesis of Ag@PPy nanocomposites, *Adv. Mater. Technol.* 3 (2018) 1700206.
- [24] S. Bellani, E. Petroni, A.E.D. Castillo, N. Curreli, B. Martín-García, R. Oropesa-Núñez, et al., Scalable production of graphene inks via wet-jet milling exfoliation for screen-printed micro-supercapacitors, *Adv. Funct. Mater.* 29 (2019) 1807659.
- [25] Z.Y. Liu, S.H. Liu, R.H. Dong, S. Yang, H. Lu, A. Narita, et al., High power in-plane micro-supercapacitors based on mesoporous polyaniline patterned graphene, *Small* 13 (2017) 1603388.
- [26] L. Liu, H.Y. Li, Y. Yu, L. Liu, Y. Wu, Silver nanowires as the current collector for a flexible in-plane micro-supercapacitor via a one-step, mask-free patterning strategy, *Nanotechnology* 29 (2018), 055401.
- [27] Z.S. Wu, K. Parvez, X.L. Feng, K. Müllen, Photolithographic fabrication of high-performance all-solid-state graphene-based planar micro-supercapacitors with different interdigital fingers, *J. Mater. Chem. A* 2 (2014) 8288–8293.
- [28] W.J. Hyun, E.B. Secor, C.H. Kim, M.C. Hersam, L.F. Franci, C.D. Frisbie, Scalable, self-aligned printing of flexible graphene micro-supercapacitors, *Adv. Energy Mater.* 7 (2017) 1700285.
- [29] C.J. Zhang, M.P. Kremer, A. Seral-Ascaso, S.H. Park, N. McEvoy, B. Anasori, et al., Stamping of flexible, coplanar micro-supercapacitors using MXene inks, *Adv. Funct. Mater.* 28 (2018) 1705506.
- [30] X.Y. Shi, F. Zhou, J.X. Peng, R.A. Wu, Z.S. Wu, X.H. Bao, One-Step scalable fabrication of graphene-integrated micro-supercapacitors with remarkable flexibility and exceptional performance uniformity, *Adv. Funct. Mater.* 29 (2019) 1902860.
- [31] Y.J. Chen, B.G. Xu, J.T. Xu, J.F. Wen, T. Hua, C.W. Kan, Graphene-based in-planar supercapacitors by a novel laser-scribing, in-situ reduction and transfer-printed method on flexible substrates, *J. Power Sources* 420 (2019) 82–87.
- [32] Y.F. Tao, C.Y.R. Wei, J.W. Liu, C.S. Deng, S. Cai, W. Xiong, Nanostructured electrically conductive hydrogels obtained via ultrafast laser processing and self-assembly, *Nanoscale* 11 (2019) 9176–9184.
- [33] H.P. Li, J.J. Liang, Recent development of printed micro-supercapacitors: printable materials, printing technologies, and perspectives, *Adv. Mater.* 32 (2020) 1805864.
- [34] X. Pu, M.M. Liu, L.X. Li, S.C. Han, X.L. Li, C.Y. Jiang, et al., Wearable textile-based in-plane micro-supercapacitors, *Adv. Energy Mater.* 6 (2016) 1601254.
- [35] R. You, Y.Q. Liu, Y.L. Hao, D.D. Han, Y.L. Zhang, Z. You, Laser fabrication of graphene-based flexible electronics, *Adv. Mater.* 32 (2020) 1901981.
- [36] L.X. Duy, Z.W. Peng, Y.L. Li, J.B. Zhang, Y.S. Ji, J.M. Tour, Laser-induced graphene fibers, *Carbon* 126 (2018) 472–479.
- [37] T.X. Tran, H. Choi, C.H. Che, J.H. Sul, I.G. Kim, S.M. Lee, et al., Laser-Induced reduction of graphene oxide by intensity-modulated line beam for supercapacitor applications, *ACS Appl. Mater. Interfaces* 10 (2018) 39777–39784.
- [38] V.G. Plotnikov, V.A. Smirnov, M.V. Alfimov, Y.M. Shul'ga, The graphite oxide photoreduction mechanism, *High Energy Chem.* 45 (2011) 411–415.
- [39] Y. Hu, H.H. Cheng, F. Zhao, N. Chen, L. Jiang, Z.H. Feng, et al., All-in-one graphene fiber supercapacitor, *Nanoscale* 6 (2014) 6448–6451.
- [40] W. Gao, N. Singh, L. Song, Z. Liu, A.L.M. Reddy, L.J. Ci, et al., Direct laser writing of micro-supercapacitors on hydrated graphite oxide films, *Nat. Nanotechnol.* 6 (2011) 496–500.
- [41] M.M. Wu, Y.R. Li, B.W. Yao, J. Chen, C. Li, G.Q. Shi, A high-performance current collector-free flexible in-plane micro-supercapacitor based on a highly conductive reduced graphene oxide film, *J. Mater. Chem. A* 4 (2016) 16213–16218.
- [42] M.F. El-Kady, V. Strong, S. Dubin, R.B. Kaner, Laser scribing of high-performance and flexible graphene-based electrochemical capacitors, *Science* 335 (2012) 1326–1330.
- [43] R. Kumar, R. Savu, E. Joanni, A.R. Vaz, M.A. Canesqui, R.K. Singh, et al., Fabrication of interdigitated micro-supercapacitor devices by direct laser writing onto ultra-thin, flexible and free-standing graphite oxide films, *RSC Adv.* 6 (2016) 84769–84776.
- [44] M.F. El-Kady, R.B. Kaner, Scalable fabrication of high-power graphene micro-supercapacitors for flexible and on-chip energy storage, *Nat. Commun.* 4 (2013) 1475.
- [45] Z.S. Wu, K. Parvez, X. Feng, K. Müllen, Graphene-based in-plane micro-supercapacitors with high power and energy densities, *Nat. Commun.* 4 (2013) 2487.
- [46] C.C. Su, C.J. Pei, B.X. Wu, J.F. Qian, Y.W. Tan, Highly doped carbon nanobelts with ultrahigh nitrogen content as high-performance supercapacitor materials, *Small* 13 (2017) 1700834.
- [47] A.C. Ferrari, J. Robertson, Interpretation of Raman spectra of disordered and amorphous carbon, *Phys. Rev. B* 61 (2000) 14095–14107.
- [48] H.A. Andreas, B.E. Conway, Examination of the double-layer capacitance of an high specific-area C-cloth electrode as titrated from acidic to alkaline pHs, *Electrochim. Acta* 51 (2006) 6510–6520.
- [49] D.H. Jurcakova, M. Seredych, G.Q. Lu, T.J. Bandosz, Combined effect of nitrogen- and oxygen-containing functional groups of microporous activated carbon on its electrochemical performance in supercapacitors, *Adv. Funct. Mater.*

- 19 (2009) 438–447.
- [50] Y.W. Zhu, S. Murali, W.W. Cai, X.S. Li, J.W. Suk, J.R. Potts, et al., Graphene and graphene oxide: synthesis, properties, and applications, *Adv. Mater.* 22 (2010) 3906–3924.
- [51] X.X. Sun, P. Cheng, H.J. Wang, H. Xu, L.Q. Dang, Z.H. Liu, et al., Activation of graphene aerogel with phosphoric acid for enhanced electrocapacitive performance, *Carbon* 92 (2015) 1–10.
- [52] E.R. Piñero, F. Leroux, F. Béguin, A high-performance carbon for supercapacitors obtained by carbonization of a seaweed biopolymer, *Adv. Mater.* 18 (2006) 1877–1882.
- [53] W.W. Liu, Y.Q. Feng, X.B. Yan, J.T. Chen, Q.J. Xue, Superior micro-supercapacitors based on graphene quantum dots, *Adv. Funct. Mater.* 23 (2013) 4111–4122.
- [54] N. Kamboj, T. Purkait, M. Das, S. Sarkar, K.S. Hazra, R.S. Dey, Ultralong cycle life and outstanding capacitive performance of a 10.8 V metal free micro-supercapacitor with highly conducting and robust laser-irradiated graphene for an integrated storage device, *Energy Environ. Sci.* 12 (2019) 2507–2517.
- [55] F. Li, M. Huang, J.H. Wang, J. Qu, Y. Li, L.X. Liu, et al., On-chip 3D interdigital micro-supercapacitors with ultrahigh areal energy density, *Energy Storage Mater.* 27 (2020) 17–24.
- [56] Y.C. Lu, Y.W. Zheng, H. Zhang, X.X. He, Q.Q. Yang, J. Wu, A high performance and flexible in-plane asymmetric micro-supercapacitor (MSC) fabricated with functional electrochemical-exfoliated graphene, *J. Electroanal. Chem.* 866 (2020) 114169.
- [57] M. Tahir, L. He, W. Yang, X.F. Hong, W.A. Haider, H. Tang, et al., Boosting the electrochemical performance and reliability of conducting polymer micro-electrode via intermediate graphene for on-chip asymmetric micro-supercapacitor, *J. Energy Chem.* 49 (2020) 224–232.
- [58] M.Z. Esfahani, M. Khosravi, Stamp-assisted flexible graphene-based micro-supercapacitors, *J. Power Sources* 462 (2020) 228166.